Kinetics of the liquid phase dehydration of 1-octanol to di-n-octyl ether on Amberlyst 70

Carlos Casas, Roger Bringué, Carles Fité, Montserrat Iborra, Javier Tejero*

Department of Chemical Engineering, Faculty of Chemistry, University of Barcelona, C/Martí i Franquès 1, 08028-Barcelona, Spain

Corresponding author: Phone: +34934021308; Fax: +34934021291; Email address: jtejero@ub.edu

Abstract

The kinetics of the liquid phase dehydration of 1-octanol to di-n-octyl ether (DNOE) over Amberlyst 70 was studied at 413-453K. Mechanistic rate models assuming water and 1-octanol adsorbed on the resin, and the free sites fraction negligible, were selected from 1-octanol dehydration experiments. Next, the influence of DNOE, water and 1,4-dioxane (solvent) concentration was evaluated. DNOE and 1,4-dioxane do not affect significantly the reaction rate, while water inhibits it strongly. Water effect was quantified by splitting the rate constant into a "true one" and a correction factor related to the fraction of active sites blocked by water. The best kinetic model stemmed from an Eley-Rideal mechanism with water adsorbed onto the resin and DNOE released directly to the liquid phase, with a correction factor for water inhibitory effect based on a Freundlich isotherm-like function; activation energy being 110±5 $kJ \cdot mol^{-1}$ based in line with literature data on homologous reactions.

Keywords

Reaction kinetics, 1-octanol dehydration, di-n-octyl ether, Amberlyst 70, reaction rate inhibition by water

Introduction

In the last two decades European oil industry is making a big effort to adapt the production facilities to maximize the production of diesel and at the same time upgrading fuel quality, as a consequence of the following factors: 1) the quick rise in diesel vehicle fleet; 2) the limits in the amounts of pollutants on exhaust gases (particulate matter, smoke, CO, NO_x, unburned hydrocarbons) set by the 98/70/EC directive;[1] 3) the severe specifications imposed by the 2003/17/EC directive involving distillation curve, cetane number, sulphur content, viscosity, density and cold flow properties; and 4) the introduction of bio-compounds in the automobile fuels composition ruled by 2009/28/EC and 2009/30/EC directives. Directive 2009/30/CE aims to reduce both the greenhouse gas emissions and the sulphur content of diesel fuels. New diesel fuel specifications set a limit value of 10 $mg \cdot kg^{-1}$ for sulphur content and a gradual reduction of life cycle greenhouse gas emissions per unit of energy from fuel and energy supplied up 10% by 31 December 2020, compared with the fuel baseline standard referred in 2010. As a result of those legislative changes, it is expected that future diesel fuels have a higher cetane index, lower density and a lower content on PAH (polycyclic aromatic hydrocarbons).[2] At this time, diesel fuel reformulation with oxygenates is a good option to upgrade the quality of diesel and comply with European standards, similarly to that of gasolines by using suitable oxygenates in the 90's.

It is well known that the addition of linear ethers containing more than nine carbon atoms to commercial gasoil upgrades the quality of the diesel blend.[3-5] Reformulated diesel fuels show higher cetane number as a result of the addition of $C_{10} - C_{16}$ linear ethers of cetane number ranging from 100 to 119; blends with linear ethers improve cold performance of commercial gasoil, and as boiling point of such ethers (from 453 to 528 K) coincides with the lower part of distillation curve of gasoil (443-633 K) its addition upgrades the vaporization of the blend. As a consequence of upgrading its quality, combustion of diesel blends is cleaner and the pollutants amount in exhaust gases decreases substantially. It is generally accepted that oxidative species will be present in the fuel during the

combustion as a result of adding compounds containing oxygen atoms to the fuel.[1] Such oxidizing agents are thought to suppress the soot formation in the early stages of its formation, what avoids its growth and agglomeration towards the formation of exhausts particulates. PAH have an important role in particulates formation as well. For this reason, PAH and soot precursors, such as benzene, must be removed. Besides, the dilution effect by the introduction of linear ethers also contributes to reduce the content of aromatic polycyclic compounds and sulphur.

Di-n-octyl ether (DNOE) is a good candidate to increase the oxygen content of diesel fuels: it has excellent cold fluid performance, blending cetane number of 119, and boiling point in the range of medium diesel fractions (Table 1). Therefore, adding DNOE to commercial diesel improves the fluid properties of blends, especially at low temperature, and their combustion since the ether avoids the formation of particles precursors. DNOE is produced by the dehydration reaction of 1-octanol. As linear primary alcohols can be obtained from hydroformylation of linear olefins, DNOE synthesis could be a way to revalue C_7 cuts from FCC. But the fact that 1-octanol could be produced from renewable sources such as bioethanol, biobutanol or glucose, is more relevant in the medium and long term. Ethanol can lead to higher linear alcohols by the Guerbert reaction on basic catalysts, i.e. ethanol dimerizes to butanol over MgO at 723 K;[7] and over nonstoichiometric hydroxyapatite at 673-723 K; 1-hexanol and 1-octanol being the main byproducts.[8,9] Moreover, Tsuchida et al. have also reported that ethanol reacts with 1-hexanol on Ca-hydroxyapatite at 611 K to give huge amounts of 1-octanol.[9] On the other hand, promising work on obtaining ethanol, butanol and octanol from sugar-derived compounds have recently shown that engineered *Escherichia coli* strain are effective at much milder experimental conditions.[10] Therefore, it is foreseen that in the near future DNOE could be obtained from biomass-derived 1-octanol in sufficient quantity, and may be labelled as biofuel.

TABLE 1

Linear symmetrical ethers are produced by the bimolecular dehydration of the respective linear 1-alkanols over acid catalysts. In general, industrial processes use sulfuric acid as catalyst.[11] Typical

disadvantages of homogeneous catalytic processes are the separation of the catalyst and product after reaction, which leads to corrosive waste streams, and furthermore the reaction product is frequently blackened by the oxidizing power of sulfuric acid.[12] A more attractive, and environmentally friendly, method for the preparation of ethers is the use of solid acid catalysts. Inorganic solid acids like η-alumina,[13] γ-alumina,[14,15] ion-exchanged montmorillonites,[16,17] and zeolites,[14,18-20] have been used in the dehydration of 1-octanol. They are not very active and, in general, favored the production of olefins above 473K (Figure 1), with the exception of H-Beta.[21] Organic acid solids like perfluoro-alkanesulfonic acids (e.g. Nafion H) and sulfonic polystyrene-co-divinylbenzene (PS-DVB) resins are able to work with high selectivity and interesting reaction rates in the temperature range 413-473K.[22,23] Nafion catalysts are quite expensive so that thermally stable PS-DVB catalysts, e.g. Amberlyst 70, are interesting catalysts to dehydrate 1-octanol to DNOE.

FIGURE 1

Previous work shows that the dehydration of 1-octanol to ether proceeds selectively (≥ 90%) under 453K with interesting reaction rates on Amberlyst 70.[23] The reaction is reversible and alcohol equilibrium conversions higher than 93% can be achieved.[24] This paper studies the kinetics of the reaction over Amberlyst70 in order to design a reactor for a potential process of DNOE synthesis.

Materials and methods

Materials

1-octanol (Acros Organics, > 99.5 pure), 1,4-dioxane (Sigma Aldrich, > 99.8% pure) and DNOE (Sigma Aldrich, > 99% pure) were used without further purification. Deionised water (resistivity 18.2 mΩ·cm) obtained in our laboratory and 1-octene (Sigma Aldrich, 99% pure) were also used.

The thermally stable ion-exchange resin Amberlyst 70 was used as the catalyst. It is a macroreticular PS-DVB ion-exchange resin with low cross-linking degree. In its synthesis, hydrogen atoms in the

polymer backbone are substituted by chlorine, and as a result the resin is thermally stable up to 473 K. The sulfonic groups (−SO_3H), which are the active sites of the catalyst, are attached to benzene rings of polymer through treatment with sulphuric acid. Its physical characteristics are gathered in Table 2.

TABLE 2

Apparatus.

Experiments were carried out in a 100 cm^3 nominal stainless steel autoclave operated in batch mode at the temperature range 413-453 K. The temperature was controlled to within ± 0.1 K by an electrical furnace. The pressure was set at 2.5 MPa by means of N_2 to maintain the liquid phase. A reactor outlet was connected directly to a sampling valve, which injected 0.1 μL of liquid into a GLC apparatus. The catalyst was injected from a pressurized vessel connected to the reactor. The reaction was controlled by a PC with a designed LabVIEW software program. Figure 2 shows a scheme of the experimental setup. More detailed information can be found elsewhere.[23]

FIGURE 2

Analysis.

Liquid samples were analysed with a HP-6890 Gas Liquid Chromatograph (GLC) equipped with TCD (thermal conductivity detector). A HP Pona methyl siloxane (HP 190915-001) capillary column (50 m length × 200 μm I.D. × 0.5 μm width of stationary phase) was used to determine 1-octene, (2Z)-2-octene, (2E)-2-octene, (3Z)-3-octene, (3E)-3-octene, 4-octene, 1-octanol, DNOE, water, and 1,4-dioxane. The column was temperature programmed with a 10 $K \cdot min^{-1}$ initial ramp from 323 to 523 K and then held for 6 min. He (30 $cm^3 \cdot min^{-1}$) was the carrier gas. All of the species were identified by using a second GLC equipped with MS (Agilent GC/MS 5973) and chemical database software.

Procedure.

Amberlyst 70 was first dried at 383 K and 101 kPa for at least 1 h, and then overnight in a vacuum oven at 1 kPa. The reactor was loaded with 70 cm^3 of 1-octanol, or 1-octanol/water/1,4-dioxane, or 1-

octanol/DNOE mixtures. The liquid was then pressurized at 2.5 MPa and warmed up to the working temperature (413-453 K). A dried sample of resin was placed in the catalyst injector, pressurized and, once the working temperature was reached, quickly shifted into the reactor with N_2 by pressure difference. The time of the catalyst injection was considered as the zero time of the experiment. Liquid samples were taken hourly to follow the reaction until the end of experiment for 6-7 h.

1-Octanol conversion (X_{OcOH}) and selectivity to DNOE with respect to 1-octanol (S_{OcOH}^{DNOE}) were defined by equations 1 and 2, respectively. DNOE formation reaction rates (r_{DNOE}) were calculated from the slope of mol DNOE produced vs. time plot and dry catalyst mass (W) by means of equation 3:

$$X_{OcOH} = \frac{Mole\ of\ 1{-}octanol\ reacted}{Mole\ of\ 1{-}octanol\ initially} \quad (1)$$

$$S_{OcOH}^{DNOE} = \frac{Mole\ of\ 1{-}octanol\ reacted\ to\ give\ DNOE}{Mole\ of\ 1{-}octanol\ reacted} \quad (2)$$

$$r_{DNOE}(t) = \frac{1}{W}\left(\frac{dn_{DNOE}}{dt}\right)_t \quad (3)$$

In all the experiments mass balance was accomplished within ± 5%. 1-Octanol conversion is accurate within ± 2-3%, and DNOE formation rates within ± 5-8%.

Results and discussion

Preliminary experiments

In order to select the operating conditions in which reaction rate is free from mass transfer effects, a number of preliminary experiments were carried out first to check the influence of the stirring speed (N) and particle size (d_p) on the reaction rate measures. Since in previous studies on the kinetics of dehydration reactions of 1-pentanol to di-n-pentyl ether (DNPE) and 1-hexanol to di-n-hexyl ether (DNHE) over Amberlyst 70 carried out in the same set up, no spurious rate measures were observed if dry catalyst mass below 3 and 4 g were used, respectively,[26,27] in the present study $W \leq 2$ g has been used to ensure that the catalyst loading is adequate to prevent deceitful rate measurements due to solid

overload in the reactor. Preliminary experiments were carried out at the highest temperature in the working range (453 K), and the maximum DNOE synthesis rate in each experiment (initial reaction rates, r^0_{DNOE}) was used for comparison, to assure that mass transfer did no influence reaction rate in the whole temperature and 1-octanol concentration ranges.

The effect of diffusion was checked by performing a series of experiments with particles of different size. Amberlyst 70 was sieved into batches of bead mean size ($d_{p,m}$) ranging from 0.12 to 0.9 mm. As Figure 3 shows, r^0_{DNOE} does not change significanty with bead size within the limits of the experimental error at a 95%-probability level. On the other hand, the influence of external mass transfer was checked in a series of experiments in which stirring speed was changed between 100 and 800 rpm, and resin samples with the commercial distribution of particle size ($d_{p,m}$ = 0.57 mm) were used. As seen in Figure 4, r^0_{DNOE} hardly changes within the limits of the experimental error at a 95%-probability level. Thus, hereinafter, experiments were performed at 500 rpm and the commercial distribution of bead sizes of Amberlyst 70 was used.

FIGURE 3; FIGURE 4

Experiments performed with 1-octanol. Kinetic study

A first series of experiments was performed processing batches of 1-octanol at different temperatures in the range 413-453 K, with a mass of dry resin of 1 or 2g. As Figure 5 shows, 1-octanol conversions increased substantially with temperature: X_{OcOH} rised from 8.9% (413K) to 60.1% (453K) with W=1g, but selectivity to DNOE decreased from 100% (413K) to 87% (453K) on increasing the temperature; octenes being the main byproduct (Figure 6).

FIGURE 5; FIGURE 6

Since alcohol-ether-water mixtures are highly non-ideal,[24,26-31] the composition of liquid mixtures is well represented by the activities of 1-octanol, DNOE and water (a_{OcOH}, a_{DNOE} and a_{H2O}, respectively), which were calculated by the UNIFAC-DORTMUND predictive method.[32] As Figures 7 to 9 show,

r_{DNOE} increased with a_{OcOH} whereas it decreased on increasing a_{DNOE} and a_{H2O}, as expected. Reaction rate is highly sensitive to temperature, and it is doubled on increasing temperature 10 K. Arrhenius plot of r^0_{DNOE} ($a_{OcOH} \approx 1$) is a good straight line in the whole temperature range (Figure 10). From the slope of the plot an apparent activation energy of 110 ± 6 kJ·mol^{-1} is estimated, in line with literature data on alcohol dehydration to linear ether over acidic resins.[26,27] This fact also backs up that r_{DNOE} measures are free from mass transfer effects at the working conditions selected

FIGURE 7; FIGURE 8; FIGURE 9; FIGURE 10

Reaction rate plots as a function of a_{OcOH}, a_{DNOE} and a_{H2O} suggest that a hyperbolic model, based on a Langmuir-Hinshelwood-Hougen-Watson (LHHW) or Eley-Rideal (ER) mechanism, might explain rate data satisfactorily. The fact that reaction rate increases with a_{OcOH} suggest that 1-octanol mainly influences the driving force of such kinetic model. The decrease of reaction rate with increasing a_{DNOE} and a_{H2O} can be attributed to the adsorption of ether and water on the resin and, as DNOE and water are reaction products, to the approach to the chemical equilibrium. Based on the analysis of the reaction rate dependence on activities, considering the adsorption-reaction-desorption process and assuming that surface reaction is the rate-limiting step, the following kinetic models were obtained:

$$r_{DNOE} = \frac{\hat{k}\prime K^2_{a,OcOH}\left[a^2_{OcOH} - \frac{a_{DNOE}\cdot a_{H_2O}}{K}\right]}{\left(1+K_{a,OcOH}\cdot a_{OcOH}+K_{a,DNOE}\cdot a_{DNOE}+K_{a,H_2O}\cdot a_{H_2O}\right)^2} \quad (4)$$

$$r_{DNOE} = \frac{\hat{k}\prime K_{a,OcOH}\left[a^2_{OcOH} - \frac{a_{DNOE}\cdot a_{H_2O}}{K}\right]}{1+K_{a,OcOH}\cdot a_{OcOH}+K_{a,DNOE}\cdot a_{DNOE}} \quad (5)$$

$$r_{DNOE} = \frac{\hat{k}\prime K_{a,OcOH}\left[a^2_{OcOH} - \frac{a_{DNOE}\cdot a_{H_2O}}{K}\right]}{1+K_{a,OcOH}\cdot a_{OcOH}+K_{a,H_2O}\cdot a_{H_2O}^2} \quad (6)$$

Equation 4 stems from a LHHW mechanism in which two 1-octanol molecules adsorbed on two adjacent sites react to give DNOE and water, both adsorbed on the resin surface.

$$1-\mathrm{OcOH}+\sigma \rightleftarrows 1-\mathrm{OcOH}\cdot\sigma$$
$$2\left(1-\mathrm{OcOH}\cdot\sigma\right) \rightleftarrows \mathrm{DNOE}\cdot\sigma+\mathrm{H_2O}\cdot\sigma$$
$$\mathrm{DNOE}\cdot\sigma \rightleftarrows \mathrm{DNOE}+\sigma$$
$$\mathrm{H_2O}\cdot\sigma \rightleftarrows \mathrm{H_2O}+\sigma$$

Equation 5 is based on an ER mechanism in which a molecule of 1-octanol from solution reacts with a molecule of 1-octanol adsorbed on an active centre to give the ether adsorbed on the resin surface, the water being released instantaneously to the liquid phase.

$$1-\mathrm{OcOH}+\sigma \rightleftarrows 1-\mathrm{OcOH}\cdot\sigma$$
$$1-\mathrm{OcOH}\cdot\sigma+1-\mathrm{OcOH} \rightleftarrows \mathrm{DNOE}\cdot\sigma+\mathrm{H_2O}$$
$$\mathrm{DNOE}\cdot\sigma \rightleftarrows \mathrm{DNOE}+\sigma$$

Equation 6 stems from an analogous ER mechanism but water remains adsorbed and the ether is released to the bulk phase.

$$1-\mathrm{OcOH}+\sigma \rightleftarrows 1-\mathrm{OcOH}\cdot\sigma$$
$$1-\mathrm{OcOH}\cdot\sigma+1-\mathrm{OcOH} \rightleftarrows \mathrm{DNOE}+\mathrm{H_2O}\cdot\sigma$$
$$\mathrm{H_2O}\cdot\sigma \rightleftarrows \mathrm{H_2O}+\sigma$$

On the basis of equations 4, 5 and 6, all possible kinetic models derived by considering negligible one or more factors of adsorption term were fitted to rate data. A detailed schedule of models handled can be found elsewhere[33]. For fitting purposes, all the models were grouped into two classes, depending on the number of free active centers (see Table 3):

(i) Class I, for which the number of free active centers is considered to be negligible compared to occupied ones. This fact implies that the unity present in the adsorption term is removed.

(ii) Class II, where that hypothesis is rejected.

TABLE 3

The number of acid sites taking part in the rate limiting step (n) is assumed that could be more than 1 or 2 since, in the case of ion exchange resins, an active site can be a group or cluster of sulfonic groups rather than an isolated one.[34] To the best of our knowledge, hyperbolic models with exponent in the denominator up to 3 are proposed often in the open literature for etherification reactions. Fité *et al.* reported that 3 active sites could take part in the rate-limiting step of ethanol addition to isobutene to yield ETBE,[35] and Solà *et al.* described ETBE synthesis through an ER mechanism with 2 active sites involved.[36] However, dehydration reactions of 1-pentanol to DNPE and 1-hexanol to DNHE proceed by means of ER mechanisms but only 1 active site is involved,[26,27] just as the reaction of 1-octanol with ethanol to yield ethyl-octyl ether reported by Guilera *et al.*[37] To achieve a good fit to rate data, n was varied from 1 to 3; n values higher than 1 for the ER mechanism, and 2 for the LHHW one, represent a scenario where additional active sites were required, for instance, to settle the long linear ether formed, or stabilize the reaction intermediate.

As seen in Table 3, the surface rate coefficient, $\hat{k}'$, and the adsorption equilibrium constants, $K_{a,OcOH}$, $K_{a,DNOE}$, and $K_{a,H2O}$, have been grouped into factors for mathematical fitting purposes, called A, B, C and D. The particular way in which those constants are grouped depends on the mechanism (LHHW or ER) and the neglected adsorption term, if any. For class I models, factor A is equal to $\hat{k}'/K_{a,OcOH}^{n-2}$ (LHHW models) or $\hat{k}'K_{a,OcOH}^{n-1}$ (ER models), whereas factors C and D are a quocient of adsorption equilibrium constants. Concerning class II models, A is equal to $\hat{k}'K_{a,OcOH}^{2}$ (LHHW models) or $\hat{k}'K_{a,OcOH}$ (ER models); B, C, and D, are the adsorption equilibrium constants of alcohol, ether and water, respectively. The temperature dependence of factors A, B, C and D was defined by:

$$A, B, C, D = \exp(a_1, b_1, c_1, d_1) \cdot \exp\left[-(a_2, b_2, c_2, d_2) \cdot \left(\frac{1}{T} - \frac{1}{\bar{T}}\right)\right] \qquad (7)$$

Therefore, fitted parameters of the models of Table 3 were *a's*, *b's*, *c's* and *d's*. The subtraction of the reverse of mean experimental temperature, $\bar{T}$ (433 K), was included to minimize the correlation

between fitted parameters (a_1 and a_2, b_1 and b_2, c_1 and c_2, d_1 and d_2, according to the respective factor). The equilibrium constant of the reaction, K, in the temperature range 413-453 K, is given by:[24]

$$K = \exp(1.7) \cdot \exp(1629/T) \quad (8)$$

To discriminate between rate models and obtain the parameters values, the sum of squares of lack of fit (RSSQ) between mesured reaction rates (r_{exp}) and those estimated by the kinetic model (r_{calc}) was minimized by the Trust-Region-Reflective Least Square method.[38,39] The objective function being:

$$\mathrm{RSSQ} = \sum_{\forall T}\left(\sum_{i=1}^{n}\left(r_{exp,i} - r_{calc,i}\right)^2\right) \quad (9)$$

Ideally, from a mathematic point of view, the most suitable model is the one with the smallest RSSQ, random residuals and low parameter correlation, or alternately low parametrical error defined as the lowest root of sum of the squares of relative errors (RSSQRE):

$$\mathrm{RSSQRE} = \left[\sum_{i=1}^{p}\left(\frac{\varepsilon_{pi}}{p_i}\right)^2\right]^{1/2} \quad (10)$$

ε_{pi} is the uncertainty of parameter p_i for a 95%-probability level (calculated by linear least squares). Besides, fitted parameters should have physicochemical meaning: rate coefficient should increase with temperature and adsorption equilibrium constant decrease, because activation energy is positive and adsorption enthalpies negative.

Kinetic models of Table 3 were fitted to reaction rate data obtained at all temperatures together. From a statistical standpoint (random residuals, minimum RSSQ and low parameter uncertainty), Class I models type 4 (coded as I-4) and type 5 (I-5) were the best (equations 11 and 12, respectively). In addition, these models have physicochemical meaning (positive activation energy)

$$r_{DNOE} = A\frac{\left[a_{OcOH}^2 - \frac{a_{DNOE}\cdot a_{H_2O}}{K}\right]}{(a_{OcOH} + C\cdot a_{DNOE})^2} \quad (11)$$

$$r_{DNOE} = A\frac{\left[a_{OcOH}^2 - \frac{a_{DNOE}\cdot a_{H_2O}}{K}\right]}{\left(a_{OcOH}+C\cdot a_{H_2O}\right)^2} \quad (12)$$

I-4 and I-5 models have similar RSSQ but uncertainty of parameters of I-5 models (with n = 1, 2 and 3) was lower than those of I-4 ones (with n = 1, 2 and 3). Parity plots (Figures S1 and S2, supplementary material) do not show significant differences when n varies from 1 to 3, but residuals dispersion of I-4 models is higher than those of I-5 ones, especially for n = 2 and 3. Values of parameters a's, c's and d's for these models are displayed in Table 4.

TABLE 4; TABLE 5

The frequency factor (A) and the activation energy (E_a) can be estimated from the values of a_1 and a_2, respectively, whereas adsorption entropy and enthalpy differences between DNOE and 1-octanol, and water and 1-octanol, can be obtained from c_1 and c_2, and d_1 and d_2 values, respectively, according to equations 11 and 12. Models I-4 and I-5 have similar frequency factor (4-5·10^{15} mol·h^{-1}·kg^{-1}) and apparent/true activation energy (120±7 kJ·mol^{-1}) as Table 5 shows. It is not possible to discern if E_a value would correspond to the true activation energy by considering the relationship between K_{OcOH} and the factor A unless the reaction mechanism (LHHW or ER) and the number of active sites involved in the rate-limiting step are previously known. Model I-5 with n=1 was the one which better fitted the kinetic data in terms of RSSQ, but the uncertainty associated to its parameters (RSSQRE) was higher than that of model I-5 with n=3. As for adsorption enthalpy and entropy differences, it is seen that adsorption of 1-octanol is more exothermic than that of water (I-5 models) and DNOE (I-4 models). The high uncertainty of c_1 and c_2, and d_1 and d_2 estimates resulted in poor adsorption entropy and enthalpy differences estimates which suggest little sensitivity of fits to factors C and D.

Effect of water and DNOE on the reaction rate

The type I-5 models showed simultaneously the smallest RSSQ and parameter uncertainty, however discriminate the best kinetic model of this group is not clear because the model with less RSSQ had greater parameter uncertainy (type I-5 with n=1) and vice versa. For this reason, a set of experiments

using 1-octanol/water and 1-octanol/DNOE mixtures was performed in order to extend the range of activities of alcohol, ether and water, and simultaneously stress the effect of DNOE and water on the reaction rate. In particular, the following set of experiments were carried out feeding:

1) 1-Octanol/DNOE mixtures (2, 4, 16, 32 and 45 wt. % DNOE at 433K, equivalent to X_{OcOH} from 0.02 to 0.47; 10 and 20 wt. % DNOE at 453 K, equivalent to X_{OcOH} = 0.11 and 0.22, respectively) to check the effect of DNOE on the reaction rate.
2) 1-octanol/1,4-dioxane/water mixtures (55 wt.% 1,4-dioxane/1, 2 and 4 wt.% water at 433K, equivalent to X_{OcOH} from 0.25 to 0.59; 55 wt.% 1,4-dioxane/0.5, 3 and 6 wt.% water at 453K, equivalent to X_{OcOH} from 0.14 to 0.69) to check the effect of water. Since 1-octanol and water are poorly miscible, 1,4-dioxane was used as a solvent in alcohol/water mixtures to prevent separation of the reaction medium into two immiscible phases, organic and aqueous. 1,4-Dioxane is a suitable solvent for alcohol-ether-water systems as it does not react with the compounds in the mixture and does not affect the morphology of Amberlyst 70 (see Table 2).[24,29]
3) 1-Octanol/1,4-dioxane mixtures (35, 45, 55 wt. % 1,4-dioxane at 423K) to check the effects of 1,4-dioxane on the reaction rate, other than dilution of liquid reaction medium.

r^0_{DNOE} vs. the initial amount of DNOE plot (Figure 11) shows that the effect of the ether on the reaction rate is not remarkable irrespective of temperature, confirming that a_{DNOE} hardly influences the term of adsorption of the rate model. The slight decrease of the initial reaction rate on increasing the initial wt. % of 1,4-dioxane (Figure 12) can be ascribed to the dilution of 1-octanol in the reaction mixture, confirming that 1,4-dioxane is a suitable solvent for this reaction system. On the contrary, as shown in Figure 13, r^0_{DNOE} decreased sharply on increasing the initial amount of water, and this effect is more noticeable as temperature rises. By comparing with rate data in the absence of water, on adding 0.5 wt.% of water r^0_{DNOE} decreases by 76% at 453K, whereas it decreases by 34% at 433K. As initial amount of water increased (4-6%), reaction rates tended to the same value (~1 $mol \cdot h^{-1} \cdot kg^{-1}$), regardless the reaction temperature. The inhibitor effect of water has been also reported in reaction systems

catalysed by ion-exchange resins other than alcohol dehydration to linear ether, as the synthesis of 4-methylpent-3-en-2-one (mesityl oxide) from acetone,[40,41] TFH production,[42] and TAME and ETBE syntheses from *tert*-amyl alcohol/methanol[43] and *tert*-butyl alcohol/ethanol mixtures,[44] respectively.

FIGURE 11; FIGURE 12; FIGURE 13

As a result of processing mixtures initially containing DNOE, water and 1,4-dioxane, the activities range of 1-octanol, DNOE and water increased, and models of Table 3 were fitted to the whole set of reaction rate data. Among thermodynamically consistent models, model I-5 with n=1 (equation 13) best represented the rate data in the entire range of activities: its RSSQ was 1301, clearly lower than that of the models I-5 with n=2 (3393) and with n=3 (17226).

$$r_{DNOE} = A \cdot \frac{\left[a_{OcOH}^2 - \frac{a_{DNOE} \cdot a_{H2O}}{K}\right]}{a_{OcOH} + D \cdot a_{H2O}} \qquad (13)$$

Factor D (= $K_{a,H2O}/K_{a,OcOH}$) estimates ranged from 0.2 (413 K) to 1.5 (453K). Although they have a high statistical uncertainty, and their values are quite different from those in the open literature (a constant value of 23 for $K_{a,H2O}/K_{a,OcOH}$ was reported in the synthesis of ethyl octyl ether from ethanol and 1-octanol over Amberlyst 70),[35] the model I-5 (n=1) suggests a scenario where water adsorption plays a more important role as temperature rises. This fact is in line with the effect of the initial water amount on r_{DNOE}^0 seen in Figure 13: the rate drop observed at 453 K, much sharper than at 433 K, suggests that water adsorption is kinetically more important as temperature increases.

Modelling the water inhibitor effect

Kinetic model I-5 (n=1) explains the inhibitory effect of water by competitive adsorption with 1-octanol. However, the inhibitory effect can be explained alternatively by the preferential adsorption of water on the acid sites, blocking them and preventing 1-octanol adsorption. Rate inhibition would be very similar to a catalyst deactivation process. With this view, an usual procedure is to modify

empirically LHHW-ER kinetic models, by splitting the rate coefficient, $\widehat{k'}$, into a "true" one, $\hat{k}'_0$, and a correction factor able to represent the rate decrease by the effect of water.[26,27,45]

A first approach was developed by Fité *et al.* in an attempt to account for the effect of the reaction medium-resin interaction on the reaction rate.[46] They proposed a correction factor, the parameter ψ, related to resin swelling and to the accessibility to resin sulfonic groups, which was useful in non-aqueous reaction media, where resins are partly swollen. However, it was not useful to explain water inhibition in the dehydration reaction of 1-alkanol to ether because the resin is not gradually swollen over the reaction, but it is fully swollen at the beginning of the reaction by the interaction of 1-alkanol and the first amounts of water released.[45] As Table 2 shows, Amberlyst 70 greatly swells in 1-octanol and water, which proves that the catalyst is completely swollen throughout the reaction of DNOE synthesis. As a consequence, this approach was discarded to explain the inhibition by water in the reaction of DNOE synthesis from 1-butanol.

A second approach was proposed by du Toit *et al.* for ion-exchange resin catalysed reactions in aqueous media, and reactions releasing water as a reaction product.[40,41] They consider that a part of the water released by reaction remains adsorbed on the resins preventing the access of reactants to the acid sites. Therefore, the rate coefficient would be proportional to the number of sites not blocked by water. As shown by Eq. 14, the correction factor is the fraction of free acid sites which depends on the water concentracion in the liquid phase and temperature, $f(a_{H2O}, T)$. As proposed by Toit *et al.*, the fraction of acid sites blocked by water molecules, θ_{H2O}, is well represented by the water adsorption isotherm. Thus, the rate coefficient can be expressed as:

$$\widehat{k'} = \hat{k}'_0 \cdot f(a_{H2O}, T) = \hat{k}'_0 \cdot (1 - \theta_{H2O}) \qquad (14)$$

Several exemples of the satisfactory use of this approach can be found in the open literature. Yang et *al*. used an inhibition term based on a Langmuir isotherm assuming adsorption of water molecules on a single site for the liquid phase synthesis of tert-amyl methyl ether from tert-amyl alcohol and

methanol,[43] and an isotherm stemming from the adsorption of two water molecules onto an active site in the synthesis of tert-amyl ethyl ether from tert-amyl ether and ethanol.[44] Limbeck at el. proposed an isotherm based on the adsorption of water onto two sites in the synthesis of THF by the cyclisation etherification of 1,4-butanediol.[42] On the other hand, du Toit et al.[41] proposed a Freundlich-like one in the acetone condensation to mesityl oxide, highlighting the inhibitory effect of water even at very small concentration**.** According to Eq. 14, some correction factors were assayed to find the best kinetic model for DNOE synthesis as shown in Table 6. Such correction factors were based on Langmuir (Eqs. 15-17) or Freundlich (Eq. 19) isotherm-like functions. Finally, a correction factor based on the adsorption of z molecules of water on an active site was also considered (Eq. 18). In equations 15-19, the adsorption equilibrium constant for water, K_{H2O}, was defined, similarly to Eq. 7, as:

$$K_{H2O} = \exp\left(K_{H2O,1}\right) \cdot \exp\left[-K_{H2O,2} \cdot \left(\frac{1}{T} - \frac{1}{\bar{T}}\right)\right] \quad (20)$$

TABLE 6

Since Eq 13 (model I-5, n=1) which contain water in the adsorption term represent accurately enough the whole set of rate data, type models of Table 3 which adsorption term does not contain water (I-1, I-2, I-4, II-1, II-2 and II-4) were fitted again to rate data by splitting the rate coefficient according to equation 14, and using the correction factors listed in Table 6. The fit of models I-2, II-2, II-4, and I-1 (n= 1 and 2) with $f(a_{H2O}, T)$ defined by equations 15 to 19, and model II-1 (n=1) with $f(a_{H2O}, T)$ defined by equations 15 to 17, resulted in either negative activation energies and/or positive adsorption enthalpies/entropies, so that these models lack physicochemical meaning, and as a consequence they were discarded.

In Figure 14, RSSQ of modified models having physicochemical meaning is compared to that of model I-5 with n=1 (equation 13), which assumes competitive adsorption of water and alcohol and does not incorporate correction factor. As seen, none of the models incorporating equations 15 and 16 as $f(a_{H2O}, T)$ improved the fit with respect to equation 13, suggesting that factors based on Langmuir

isotherms where more than a water molecule is adsorbed on an active site are more suitable. In this way, when equations 17-19 were used as $f(a_{H2O}, T)$, RSSQ was lower than that of equation 13. As seen, modified models II-2 with n=2 and 3 had the lowest RSSQ, but activation energy estimates were too low (20-70 kJ·mol^{-1}) compared with those of analogous reactions of alcohols dehydration, and also with the value of 110±6 kJ·mol^{-1} found from r^0_{DNOE} values (section 3.2). Rate equations stemming from models I-1 (n=1) and I-4 (n=1), and include the correction factors defined by equations 17-19, show similar RSSQ. Therefore, modified I-1 model was selected since they have two less parameters than the models of the group I-4.

FIGURE 14; TABLE 7

As shown in Table 7, the correction factors defined by equations 17-19 greatly improve the fit of model I-1 (n=1) since RSSQ decreases by 75-78%. In addition, the modified models have lower RSSQ and parameter uncertainty (RSSQRE) than model I-5(n=1) (equation 13). Equation 17 is based on a Langmuir isotherm-like where two molecules of water adsorb on an active site. Equation 18 considers the number of molecules of water adsorbed (z) in a single active site as a parameter to fit. Model I-1 (n=1) modified by this correction factor sets z=3.2 water molecules adsorbed each active site. Despite, z is strictly an empiric parameter; its value is close to the one found in resin drying experiments.[47,48] However, a correction factor based on a Freundlich isotherm-like function led to the smallest RSSQ (962) having the same number of parameters to fit. For this reason, model I-1 (n=1) with a correction factor defined by equation 19 was selected as the best model to represent the whole series of rate data of DNOE synthesis, whose final form is:

$$r_{DNOE} = \frac{A\cdot\left[a^2_{OcOH} - \frac{a_{DNOE}\cdot a_{H2O}}{K}\right]}{a_{OcOH}} \cdot \left[1 - K_{H2O} a^{1/\alpha}_{H2O}\right] \qquad (21)$$

with $A = exp(2.79)\cdot exp\left[-1.34\cdot 10^4 \cdot \left(\frac{1}{T} - \frac{1}{\bar{T}}\right)\right]$

and $K_{H2O} a^{1/\alpha}_{H2O} = K_{H2O} a^{T/K_\alpha}_{H2O} = \exp(0.5)\cdot\exp\left[-3\cdot 10^3 \cdot \left(\frac{1}{T} - \frac{1}{\bar{T}}\right)\right] a^{T/272}_{H2O}$

The parity plot (Figure 15) shows that equation 21 well represents rate data as a whole, but in some experiments with low water content in the feed performed at 453K.

FIGURE 15; TABLE 8

According to equation 21 dehydration of 1-octanol to DNOE follows an Eley-Rideal mechanism where a molecule of 1-octanol adsorbed on a site reacts with a molecule of 1-octanol from the liquid phase. A first effect of introducing $f(a_{H2O}, T)$ as correction factor, and so finding the true rate coefficient is that activation energy decreases with regard to those of models I-4 and I-5 (120±7 kJ·mol^{-1}). Activation energy for equation 21 is 110±5 kJ·mol^{-1}, the same value found from the r^0_{DNOE} Arrhenius plot which proves that interaction of equation 21 parameters is low. As Table 8 shows, this value is a bit smaller that those of the reactions of dehydration of butanol to di-n-butyl ether (DNBE, 122±2 kJ·mol^{-1}),[49] of pentanol to DNPE (114±0,1 kJ·mol^{-1}),[26] and hexanol to DNHE (121±3 kJ·mol^{-1}),[27] respectively, on Amberlyst 70. On the other hand, in the dehydration of ethanol and 1-octanol to ethyl octyl ether, DNOE synthesis is a side reaction with similar activation energy on Amberlyst 70 (99 kJ·mol^{-1}) and on CT-482 (100 kJ·mol^{-1}).[50] Finally, activation energy is lower than on H-beta (150±12 kJ·mol^{-1}) showing that Amberlyst 70 is more active in the temperature range explored

FIGURE 16

Figure 16 plots the values of the correction factor, $1 - K_{H_2O} a_{H_2O}^{1/\alpha}$, as used in equation 21 versus a_{H_2O} in the whole temperature range. The correction factor decreases on increasing the temperature and a_{H_2O}, therefore its effect is higher. It is to be noted that trends of correction factor and r_{DNOE} are similar for experiments processing 1-octanol feed wherein water is released. In this way, an amount of water equivalent to a_{H_2O} between 0.6 at 453K and 0.8 at 413K inhibits practically the reaction (see Figure 9). However the trends of correction factor and r_{DNOE} are alike for $a_{H_2O} \leq 0.25$ in the experiments containing water initially since Figure 13 shows that for larger a_{H_2O} values, r_{DNOE} tend to a plateau which hardly changes with the initial water content, whereas the correction factor decreases

monotonically. This could be because Freundlich isotherm is usually valid for low and intermediate especies activities.

On the other hand, the Freundlich isotherm approach expects that α decreases almost linearly with temperature and K_{H_2O} is non-dependent.[40,51] Moreover, α should be larger than one. From values of $K_{\infty}, K_{H_2O,1}$ and $K_{H_2O,2}$ (Table 7) it is seen that (a) α decreases with temperature and it is lower than unity, and (b) K_{H_2O} at 453K is nearly twice that at 413K. Accordingly, $f(a_{H2O}, T) = 1 - K_{H_2O} a_{H_2O}^{1/\alpha}$, decreases with temperature for the same a_{H2O} value. These points suggests the the fitting improvement is due to the flexibility of the power expression for $\theta_{H_2O}$and to the fact that equation 21 involved more parameters rather than to a fundamental insight of the Freundlich isotherm-like function. Thus, the kinetic model (equation 21) is a pseudo-empirical model rather than a mechanistic one. However, if the correction factor is considered in terms of catalyst deactivation, K_{H_2O} can be considered as a deactivation constant. Consequently, from its temperature dependence a pseudoactivation energy for the water deactivation process of 25 kJ·mol^{-1} could be computed.

FIGURE 17

Correction factors based on the Freundlich isotherm has been successfully used to explain inhibition by water in the acetone dehydration to mesityl oxide on Amberlyst 16,[40,41] and in the dehydration reaction of 1-alkanol to linear symmetrical ether on Amberlyst 70.[26,27,45,49] Figure 17 compares the correction factors, $1 - K_{H_2O} a_{H_2O}^{1/\alpha}$, for the dehydration reactions of 1-pentanol to DNPE,[26,45] 1-hexanol to DNPE[27] and 1-butanol to di-n-butyl ether (DNBE)[49] at 443K found in our previous works. As seen, the inhibitory effect of water on the reaction rate is quite similar for the reactions of synthesis linear ether. The correction factor have similar values for low a_{H_2O} values, but they are quite different at high activity values according to its empirical character. However, in all those reactions reaction rate is well reprented and the inhibitory effect of water satisfactorily predicted, showing that even moderate amounts of water in the liquid phase could stop the reaction. Finally, as a consequence of the decisive

role of water in these reactions, in industrial practice it is advisable using reaction devices which allow removing water as it is formed

Conclusions

The kinetics of the liquid phase dehydration of 1-octanol to DNOE over Amberlyst 70 was studied at 413-453 K and 2.5 MPa. Experiments were performed in a stirred tank reactor free of mass transfer limitation by working with 1-2 g of catalyst (commercial distribution of bead sizes) and stirring speed 500 rpm. Kinetic equations based on LHHW-ER mechanisms were obtained by assuming that surface reaction was the rate-limiting step and fitted to rate data. Analysis of experiments performed with pure 1-octanol revealed that models where 1-octanol and water adsorb preferentially on the resin and the fraction of free active sites is negligible were the best ones. Apparent activation energies of 120±7 $kJ \cdot mol^{-1}$ were estimated for these models. Water, DNOE and solvent (1,4-dioxane) influence on the reaction rate was then evaluated. DNOE and 1,4-dioxane did not show significant effects on the reaction rate whereas water strongly inhibited the reaction rate. Its inhibitor effect can be explained by competitive adsorption of water and 1-octanol, or else by blocking of active sites by water. On the last assumption, since reaction rate is proportional to the number of accessible acid sites, LHHW-ER mechanistic models were modified by splitting off the rate coefficient into a "true" one and the fraction of active sites not blocked by water. The fraction of free acid sites is described by Langmuir or Freundlich isotherm-like functions. The best reaction model for the reaction of DNOE synthesis by 1-octanol dehydration is based on an Eley-Rideal mechanism in which one molecule of 1-octanol adsorbed onto the resin reacts with another molecule of 1-octanol of the liquid phase; the deactivation-like effect of water is satisfactorily represented by a Freundlich isotherm-like function. Activation energy estimated by fitting this model to the whole series of rate data was 110±5 $kJ \cdot mol^{-1}$.

Acknowledgements

Authors thank to State Education, Universities, Research & Development Office of Spain for financial support (Projects CTQ2007-60691/PPQ and CTQ2010-16047). The authors also thank Rohm and Haas for supplying ion exchange resin Amberlyst 70.

Nomenclature

A	Frequency factor, $mol \cdot h^{-1} \cdot kg^{-1}$
A, B, C, D	Grouped factors for fitting purposes
a_1, b_1, c_1, d_1	First fitting parameter of factors A, B, C and D
a_2, b_2, c_2, d_2	Second fitting parameter of factors A, B, C and D, K
a_j	Activity of compound j
d_p	Particle diameter, mm
$d_{p,m}$	Mean particle diameter, mm
E_a	Activation energy, $kJ \cdot mol^{-1}$
$f(a_{H2O})$	Correction factor for water inhibition effect
K	Chemical equilibrium constant
K_α	Freundlich parameter, K
$K_{a,j}$	Adsorption equilibrium constant of compound j
K_{H2O}	Adsorption equilibrium constant of water
$K_{H2O,1}$	First fitting parameter of K_{H2O}
$K_{H2O,2}$	Second fitting parameter of K_{H2O}, K
$\hat{k}'$	Surface reaction rate coefficient, $mol \cdot h^{-1} \cdot kg^{-1}$
$\hat{k}'_0$	"True" surface reaction rate coefficient, $mol \cdot h^{-1} \cdot kg^{-1}$
N	Stirring speed, rpm
n	Number of active centres involved in the chemical reaction
n_{DNOE}	Number of moles of DNOE, mol

p_i	Fitting parameter i
r_{calc}	Reaction rate computed by a rate model, $mol \cdot h^{-1} \cdot kg^{-1}$
r_{exp}	Reaction rate obtained from experimens, $mol \cdot h^{-1} \cdot kg^{-1}$
r_{DNOE}	DNOE formation rate, $mol \cdot h^{-1} \cdot kg^{-1}$
r^0_{DNOE}	Initial reaction rate of DNOE formation, $mol \cdot h^{-1} \cdot kg^{-1}$
S_{BET}	Surface area estimated by Brunauer-Emmett-Teller (BET) method, $m^2 \cdot g^{-1}$
S_{area}	Surface area estimated from ISEC data, $m^2 \cdot g^{-1}$
S_{OcOH}^{DNOE}	Selectivity to DNOE with regard to 1-octanol
T	Temperature, K
$\bar{T}$	Mean temperature, K
t	Time, h
W	Dry catalyst mass, kg
X_{OcOH}	1-Octanol conversion
$\Delta H_{a,j}$	Adsorption enthalpy of compound j, $kJ \cdot mol^{-1}$
$\Delta S_{a,j}$	Adsorption entropy of compound j, $J \cdot mol^{-1} \cdot K^{-1}$

Greek symbols

α	Fitting parameter in Freundlich isotherm
ε_p	Uncertainty of p_i
θ	Catalyst porosity, %
θ_{H2O}	Fraction of active sites blocked by water
ρ_s	Skeletal density, $g \cdot cm^{-3}$
σ	Active site

Abbreviations

BuOH	1-butanol
DNBE	Di-n-butyl ether

DNHE	Di-n-hexyl-ether
DNOE	Di-n-octyl-ether
DNPE	Di-n-pentyl-ether
HeOH	1-hexanol
ISEC	Inverse steric exclusion chromatography
LHHW-ER	Langmuir Hinshelwood Hougen Watson-Eley Rideal
OcOH	1-Octanol
PeOH	1-Pentanol
PS-DVB	Polystyrene-co-divinylbenzene polymer.
RSSQ	Residual sum of squares
RSSQRE	Root of sum of squares of relative errors

References

1. Nylund NO, Aakko P, Niemi S, Paanu T, Berg R. Alcohols/ethers as oxygenates in diesel fuel: Properties of blended fuels and evaluation of practical experiences. Annex XXVI of the 27th meeting of IEA Implementing Agreement on Advanced Motor Fuels. Report TEC 3/2005.

2. Pöttering HG, Necas P. Directive 2009/30/EC of the European parliament and of the Council of 23 April 2009 amending Directive 98/70/EC as regards the specification of petrol, diesel and gas-oil introducing a mechanism to monitor and reduce greenhouse gas emissions and amending Council Directive 1999/32/EC as regards the specification of fuel used by inland waterway vessels and repealing Directive 93/12/EC. *Off. J. Eur. Union* 2009;140:88-112.

3. Pecci GC, Clerici MG, Giavazzi F, Ancilloti F, Marchionna M, Patrini R. Oxygenated diesel fuels. Part 1 Structures and properties correlation. *Int Symp Alcohol Fuels* 1991;1:321-326.

4. Marchionna M, Patrini R, Giavazzi F, Pecci GC. Linear ethers as high quality components for diesel fuels. *Abstract of papers Am Chem Soc*. 1996;212:PETR 24.

5. Olah GA inventor; Olah GA assignee. Cleaner burning and cetane enhancing diesel fuel supplements. US Patent 5520710, May 28, 1996.

6. Reinish J, Klamt A. Predicting flash points of pure compounds and mixtures with COSMO-RS. *Ind Eng Chem Res.* 2015;54:12974-12980

7. Ndou AS, Plint N, Coville NJ. Dimerisation of ethanol to butanol over solid-base catalysts. *App Catal A. Gen*. 2003;251:337-345

8. Tsuchida T, Sakuma S, Takeguchi T, Ueda W. Direct synthesis of n-butanol from ethanol over nostoichiometric hydroxyapatite. *Ind Eng Chem Res*. 2006;45:8634-8642

9. Tsuchida T, Yoshioka T, Sakuma S, Takeguchi T, Ueda W. Synthesis of biogasoline from ethanol over hydroxyapatite catalysts. *Ind Eng Chem Res*. 2008;47:1443-1452

10. Kremer F, Blank LM, Jones PR, Akhtar MK. A comparison of the microbial production and combustion characteristics of three alcohol biofuels: ethanol, 1-butanol, and 1-octanol. *Frontiers in Bioengineering and Biotechnology* 2015;3:112

11. Norris JF, Rigby GW. The reactivity of atoms and groups in organic compounds. XII. The preparation and properties of mixed aliphatic ethers with special reference to those containing the tert.-butyl radical. *J. Am Che. Soc*. 1932;54:2088-2100

12. Patrini R, Marchionna M. UK Patent Application GB 2.323.844 A. 1998

13. Nel RJJ, de Klerk A. Dehydration of C_5-C_{12} linear 1-alcohols over η-alumina to fuel ethers. *Ind Eng Chem Res.* 2009;48:5230-5238

14. Palla VChS, Shee D, Maity SK. Kinetics of hydrodeoxygenation of octanol over supported nickel catalysts: a mechanistic study. *RSC Advances.* 2014;4:41612-41621

15. Makgoba NP, Sakuneka TM, Koortzen JG, Van Schalkwyk C, Botha JM, Nicolaides CP. Silication of γ-alumina catalysts during the dehydration of linear primary alcohols. *Appl Catal A: Gen*. 2006;297:145-150

16. Ballantine JA, Davies M, Patel I, Purnell JH, Rayanakorn M, Williams KJ, Thomas JM. Organic reactions catalysed by sheet silicates: ether formation by the intermolecular dehydration of alcohols and by the addition of alcohols to alkenes. *J. Mol Catal*. 1984;26:37-56

17. Ballantine JA, Davies M, Purnell H, Rayanajorn M, Thomas JM, Williams KJ. Chemical conversions using sheet silicates: novel intermolecular dehydrations of alcohols to ethers and polymers. *J. Am Soc Chem Commun.* 1981;9:427-428

18. Hoek I, Nijhuis TA, Stankiewicz AI, Moulijn JA. Kinetics of solid acid catalysed etherification of symmetrical primary alcohols: zeolite BEA catalysed etherification of 1-octanol. *Appl Cata. A: Gen.* 2004;266:109-116

19. Dimitri OIH, Sultan EA. A study on catalytic conversion of alcohols over ion-exchanged molecular sieve zeolite catalyst. *Delta J. Science* 1990;14:540-557

20. Todd AD, Bielanski CW. Graphite oxid activated zeolite NaY: applications in alcohol dehydration. *Cat Sci Tech.* 2013;3:135-139

21. Casas C, Bringué R, Ramírez E, Iborra M, Tejero J. Deshidratación de 1-octanol sobre zeolitas y resinas de intercambio iónico. *Ingeniería Química* 2010;494;70-74

22. Olah GA, Shamma T, Surya Prakash GK. Dehydration of alcohols to ethers over Nafion-H a solid perfluoroalkanesulfonic acid resin catalyst. *Catal. Letters* 1997;46:1-4.

23. Casas C, Bringué R, Ramírez E, Iborra M, Tejero J. Liquid-phase dehydration of 1-octanol, 1-hexanol and 1-pentanol to linear symmetrical ethers over ion exchange resins. *Appl Catal A: Gen*. 2011;396:129-139.

24. Casas C, Fité C, Iborra M, Tejero J, Cunill F. Chemical equilibrium of the liquid-phase dehydration of 1‑octanol to 1‑(octyloxy)octane. *J. Chem Eng Data* 2013;52:741-748.

25. Fisher S, Kunin R. Routine exchange capacity determinations of ion exchange resins. *Anal Chem.* 1955;27:1191-1194.

26. Bringué R, Ramírez E, Fité C, Iborra M, Tejero J. Kinetics of 1-pentanol etherification without water removal. Ind. Eng. Chem. Res. 2011;50:7911-1919.

27. Bringué R, Ramírez E, Iborra M, Tejero J, Cunill F. Kinetics of 1-hexanol etherification on Amberlyst 70. *Chem Eng J*. 2014;246:71-78

28. Bringué R, Tejero J, Iborra M, Izquierdo JF, Fité C, Cunill F. experimental study of the chemical equilibria in the liquid-phase dehydration of 1-pentanol to di-n-pentyl Ether. *Ind Eng Chem Res.* 2007;46;6865-6872

29. Bringué R, Tejero J, Iborra M, Fité C, Izquierdo JF, Cunill F. Study of the chemical equilibrium of the liquid-phase dehydration of 1-hexanol to dihexyl ether. *J. Chem Eng Data* 2008;53:2854-2860

30. Graça NS, Pais LS, Silva VMTM, Rodrigues AE. Oxygenated biofuels from butanol for diesel blends: synthesis of the acetal 1,1-dibutoxyethane catalyzed by Amberlyst-15 ion-exchange resin. *Ind. Eng. Chem. Res.* 2010;49:6763-6771

31. Silva VMTM, Rodrigues AE. Kinetic studies in a batch reactor using ion exchange resin caralysts for oxygenates production: role of mass transfer machanisms. *Chem. Eng. Sci.* 2006;61: 316-331

32. Witting R, Lohmann J. Vapor-liquid equilibria by UNIFAC group contribution. 6. Revision and extension. *Ind Eng Chem Res*. 2003;42:183-188.

33. Tejero J, Cunill F, Iborra M, Izquierdo JF, Fité C, Bringué R. Liquid-phase dehydration of 1-pentanol to di-n-pentyl ether (DNPE) over medium and large pore acidic zeolites. *Micro Meso Materials* 2009;117:650-660.

34. Buttersack C, Widdecke J, Klein J. The concept of variable active centers in acid catalysis: part I. Alkylation of benzene with olefins catalyzed by ion-exchange resins. *J. Mol. Catal*. 1986;38: 365-381.

35. Fité C, Iborra M, Tejero J, Izquierdo JF, Cunill F. Kinetics of the liquid-phase synthesis of ethyl tert-butyl ether (ETBE). *Ind Eng Chem Res***.** 1994;33:581-591.

36. Solà L, Pericàs MA, Cunill F, Tejero J. Thermodynamic and kinetic studies of the liquid-phase synthesis of tert-butyl ethyl ether using a reaction calorimeter. *Ind Eng Chem Res*. 1995;34:3718-3725.

37. Guilera J, Bringué R, Ramírez E, Fité C, Tejero J. Kinetic study of ethyl octyl ether formation from ethanol and 1-octanol on Amberlyst 70. *AIChE Journal* 2014**;**60:2918-2928

38. Coleman TF, Li Y. An interior trust region approach for nonlinear minimization subject to bounds. *SIAM J. Optimization* 1996;*6:*418-445.

39. Coleman TF, Li Y. On the convergence of reflective Newton methods for large-scale nonlinear minimization subject to bounds. *Mathematical Programing* 1994;67:189-224

40. du Toit E, Nicol W. The rate inhibiting effect of water as a product on reactions catalyzed by cation exchange resins: formation of mesityl oxide from acetone as case study. *App Catal A: Gen*. 2004;277:219-225.

41. du Toit E, Schwarzer R, Nicol W. Acetone condensation on a cation exchange resin catalyst: the pseudo equilibrium phenomenon. *Chem. Eng. Sci*. 2004;59:5545-5550.

42. Limbeck U, Altwicker C, Kunz U, Hoffmann U. Rate expression for TFH synthesis on acidic ion exchange resin. *Chem. Eng. Sci*. 2001**;**56:2171-2178

43. Yang B, Maeda M, Goto S. Kinetics of liquid synthesis of tert-amyl methyl ether from tert-amyl alcohol and methanol catalyzed by ion exchange resin. *J. Chem. Kinet*. 1997;30:137-143.

44. Yang B, Yang S, Yao R. Synthesis of ethyl tert-butyl ether from tert-butyl alcohol and ethanol on strong acid cation-exchange resins. *React. Funct. Polym*. 2000;44:167-175.

45. Bringué R, Tejero J, Iborra M, Izquierdo JF, Fité C, Cunill F. Water effect on the kinetics of 1-pentanol dehydration to di-n-pentyl ether (DNPE) on Amberlyst 70. *Top. Catal* 2007; 45:181-186

46. Fité C, Tejero J, Iborra M, Cunill F, Izquierdo JF. Enhancing MTBE rate equation by considering reaction medium influence. *AIChE Journal* 1998;44:2273-2279

47. Iborra M, Fité C, Tejero J, Cunill F, Izquierdo JF. Drying of acidic macroporous styrene-divinylbenzene resins. *React. Polym*. 1993;21:65-76.

48. Iborra M, Tejero J, Cunill F, Izquierdo JF, Fité C. Drying of acidic macroporous styrene-divinylbenzene resins with 12-20% cross-linking degree. *Ind Eng Chem Res*. 2000;39:1416-1422.

49. Pérez-Maciá MA, Bringué R, Iborra M, Tejero J, Cunill F. Kinetic study of 1-butanol dehydration to di-n-butyl ether over Amberlyst 70, *AIChE Journal* 2016;62:180-194.

50. Guilera J, Ramírez E, Fité C, Iborra M, Tejero J. Thermal stability and wáter effect on ion-exchange resins in ethyl ether production at high temperature. Appl Catal A: Gen. 2013; 467:301-309

51. Adamson AW, Physical Chemistry of Surfaces (Fifth edidion), New York: Wiley, 1990, pp 421-426

FIGURE CAPTIONS

Figure 1. Reaction scheme in the dehydration of 1-octanol to DNOE

Figure 2. Experimental Setup

Figure 3. Influence of bead size on initial DNOE formation rate. (70 cm^3 1-octanol, W = 1 g, T = 453 K, N = 500 rpm). Error bars indicate the confidence interval at a 95%-probability level.

Figure 4. Influence of stirring speed (N) on initial DNOE formation rate (70 cm^3 1-octanol, W = 1 g, $d_{p,m}$ = 0.57 mm, T = 453 K). Error bars indicate the confidence interval at a 95%-probability level.

Figure 5. 1-Octanol conversion against contact time. 70 $cm^3$of 1-octanol, W = 1-2 g, $d_{p,m}$ = 0.57 mm, N =500 rpm, W = 1 (solid symbols) or 2 (open symbols) g.

Figure 6. Selectivity to DNOE vs. conversion of 1-octanol. 70 $cm^3$of 1-octanol, W = 1-2 g, $d_{p,m}$ = 0.57 mm, N =500 rpm, W = 1 (solid symbols) or 2 (open symbols) g.

Figure 7. Reaction rates of DNOE formation vs. 1-octanol activity at 413 K (+), 423 K (■), 433 K (♦), 443 K (▲), 453 K (●). 70 $cm^3$of 1-octanol, W = 1-2 g, $d_{p,m}$ = 0.57 mm, N =500 rpm.

Figure 8. Reaction rates of DNOE formation vs. DNOE activity at 413 K (+), 423 K (■), 433 K (♦), 443 K (▲), 453 K (●). 70 $cm^3$of 1-octanol, W = 1-2 g, $d_{p,m}$ = 0.57 mm, N =500 rpm.

Figure 9. Reaction rates of DNOE formation vs. water activity at 413 K (+), 423 K (■), 433 K (♦), 443 K (▲), 453 K (●). 70 $cm^3$of 1-octanol, W = 1-2 g, $d_{p,m}$ = 0.57 mm, N =500 rpm.

Figure 10. Arrhenius plot for initial DNOE formation rate (W = 1-2 g, $d_{p,m}$ = 0.57 mm, T = 413-453 K, N = 500 rpm).

Figure 11. Influence of initial DNOE amount (% wt) on initial reaction rate of DNOE formation at 453K (■) and 433K (●) (70 cm^3 of 1-octanol/DNOE mixture, W = 1 g, $d_{p,m}$ = 0.57 mm, N = 500 rpm). Error bars indicate the confidence interval at a 95%-probability level

Figure 12. Effect of 1,4-dioxane amount (wt%) on initial reaction rate of DNOE formation at 423K (70 cm^3 1-octanol/1,4-dioxane mixture, W = 1 g, $d_{p,m}$ = 0.57 mm, N = 500 rpm). Error bars indicate the confidence interval at a 95%-probability level

Figure 13. Influence of initial water amount (% wt) on initial reaction rate of DNOE formation at 453K (■) and 433K (●) (70 cm^3 1-octanol/water/1,4-dioxane mixtures, W = 1 g, $d_{p,m}$ = 0.57 mm, N = 500 rpm). Error bars indicate the confidence interval at a 95%-probability level

Figure 14. RSSQ for model I-5 with n=1, equation 13 (▬), and models I-1 with n=1 (■), II-1 with n=1 (■) n=2 (■) and n=3 (dotted bar), and I-4 with n=1 (□) with correction factors for inhibitor effect of water based on equations 15-19

Figure 15. Parity plot for equation 21 (♦, experiments processing only OcOH; o, OcOH-DNOE blends; •, 1,4-dioxane/OcOH/water blends; +, 1,4-dioxane/OcOH blends)

Figure 16. Correction factor for the inhibitory effect of water based on the Freundlich isotherm vs. water activity at different temperatures within the range 413-453K.

Figure 17. Correction factor for the inhibitory effect of water based on the Freundlich isotherm vs. a_{H2O} in the reactions of synthesis of DNBE, DNPE, DNHE and DNOE, respectively, by dehydration of 1-alkanol at 443 K.

Table 1. Specifications for market fuels to be used for diesel fueled vehicles in force in Europe since 2010 after the implementation of the directive 2009/30/EC,[2] and properties of DNOE as diesel fuel.[3]

Parameter	Diesel fuel		DNOE
	Minimum	Maximum	
Cetane number	51		119
Density at 288K, $kg \cdot m^{-3}$	820	845	807
Boiling point, K			559
Distillation:			
- 65% v/v recovered, K	523		
- 85% v/v recovered, K		623	
- 95% v/v recovered, K		633	
Polycyclic aromatic hydrocarbons, % w/w		8.0	
Sulphur content, $mg \cdot kg^{-1}$		10.0	
Flash point, K	328		412[a]
Cloud point (CP), K	263	273	256
Cold flow plugging point (CFPP), K	263	273	258

a) Estimated by means of COSMO-RS.[6]

Table 2. Physical and morphological properties of Amberlyst 70

Catalyst	Amberlyst 70
Structure	Macroreticular
Divinylbenzene (%)	7-8
Chlorinated	Yes
Sulfonation type	Monosulfonated
Skeletal density, ρ_s ($g \cdot cm^{-3}$)[a]	1.52
Acid capacity (mol $H^+ \cdot kg^{-1}$) [b]	2.65
Maximum operating temperature (K)	463
In dry state	
Mean particle size, $d_{p,m}$ (mm)[c]	0.57
Surface area ($m^2 \cdot g^{-1}$)[d]	0.02
Pore volume ($cm^3 \cdot g^{-1}$)[d]	0.0
Porosity, θ (vol. %)	0.00
In water swollen state	
Mean particle size, $d_{p,m}$ (mm)[c]	0.86
Surface area ($m^2 \cdot g^{-1}$)[e]	176
Pore volume ($cm^3 \cdot g^{-1}$)[e]	0.36
Volume of the swollen polymer phase, V_{sp} ($cm^3 \cdot g^{-1}$)[e]	1.40
Porosity, θ (vol. %)	62.5
Swelling (%)	243
In 1-octanol swollen state	
Mean particle size, $d_{p,m}$ (mm)[c]	0.84
Swelling (%)	220
In 1,4-dioxane	
Mean particle size, $d_{p,m}$ (mm)[c]	0,56

[a]Determined by helium displacement

[b]Determined by titration against standard base following the Fischer-Kunin method[25]

[c]Determined by laser diffraction

[d]From N_2 adsorption-desorption at 77 K. Surface area by BET method. Pore volume from adsorption data at 99% relative pressure

[e]From analysis of Inverse Steric Exclusion Chromatografy (ISEC) data in aqueous media

Table 3. Kinetic models fitted with n ranging from 1 to 3

Type	CLASS I	CLASS II
1	$r_{DNOE} = \frac{A \cdot \left[a_{OcOH}^2 - \frac{a_{DNOE} \cdot a_{H2O}}{K}\right]}{(a_{OcOH})^n}$	$r_{DNOE} = \frac{A \cdot \left[a_{OcOH}^2 - \frac{a_{DNOE} \cdot a_{H2O}}{K}\right]}{(1 + B \cdot a_{OcOH})^n}$
2	$r_{DNOE} = \frac{A \cdot \left[a_{OcOH}^2 - \frac{a_{DNOE} \cdot a_{H2O}}{K}\right]}{(a_{DNOE})^n}$	$r_{DNOE} = \frac{A \cdot \left[a_{OcOH}^2 - \frac{a_{DNOE} \cdot a_{H2O}}{K}\right]}{(1 + C \cdot a_{DNOE})^n}$
3	$r_{DNOE} = \frac{A \cdot \left[a_{OcOH}^2 - \frac{a_{DNOE} \cdot a_{H2O}}{K}\right]}{(a_{H2O})^n}$	$r_{DNOE} = \frac{A \cdot \left[a_{OcOH}^2 - \frac{a_{DNOE} \cdot a_{H2O}}{K}\right]}{(1 + D \cdot a_{H2O})^n}$
4	$r_{DNOE} = \frac{A \cdot \left[a_{OcOH}^2 - \frac{a_{DNOE} \cdot a_{H2O}}{K}\right]}{(a_{OcOH} + C \cdot a_{DNOE})^n}$	$r_{DNOE} = \frac{A \cdot \left[a_{OcOH}^2 - \frac{a_{DNOE} \cdot a_{H2O}}{K}\right]}{(1 + B \cdot a_{OcOH} + C \cdot a_{DNOE})^n}$
5	$r_{DNOE} = \frac{A \cdot \left[a_{OcOH}^2 - \frac{a_{DNOE} \cdot a_{H2O}}{K}\right]}{(a_{OcOH} + D \cdot a_{H2O})^n}$	$r_{DNOE} = \frac{A \cdot \left[a_{OcOH}^2 - \frac{a_{DNOE} \cdot a_{H2O}}{K}\right]}{(1 + B \cdot a_{OcOH} + D \cdot a_{H2O})^n}$
6	$r_{DNOE} = \frac{A \cdot \left[a_{OcOH}^2 - \frac{a_{DNOE} \cdot a_{H2O}}{K}\right]}{(a_{DNOE} + D \cdot a_{H2O})^n}$	$r_{DNOE} = \frac{A \cdot \left[a_{OcOH}^2 - \frac{a_{DNOE} \cdot a_{H2O}}{K}\right]}{(1 + C \cdot a_{DNOE} + D \cdot a_{H2O})^n}$
7	$r_{DNOE} = \frac{A \cdot \left[a_{OcOH}^2 - \frac{a_{DNOE} \cdot a_{H2O}}{K}\right]}{(a_{OcOH} + C \cdot a_{DNOE} + D \cdot a_{H2O})^n}$	$r_{DNOE} = \frac{A \cdot \left[a_{OcOH}^2 - \frac{a_{DNOE} \cdot a_{H2O}}{K}\right]}{(1 + B \cdot a_{OcOH} + C \cdot a_{DNOE} + D \cdot a_{H2O})^n}$

Relation between factors A, B, C and D, and rate coefficient and adsorption equilibrium constants

Model Type	A (LHHW)	A (ER)	B	C	D
CLASS I	$\hat{k}'/K_{a,OcOH}^{n-2}$	$\hat{k}'/K_{a,OcOH}^{n-1}$		$K_{a,DNOE}/K_{a,OcOH}$	$K_{a,H2O}/K_{a,OcOH}$
CLASS II	$\hat{k}'K_{a,OcOH}^2$	$\hat{k}'K_{a,OcOH}$	$K_{a,OcOH}$	$K_{a,DNOE}$	$K_{a,H2O}$

Table 4. RSSQ and RSSQRE of I-4 and I-5 models, and values of parameters a_1, a_2, c_1, c_2, d_1 and d_2.

Model type	n	RSSQ	RSSQRE	a_1	$a_2 \cdot 10^{-4}$	$c_1 \cdot 10$	$c_2 \cdot 10^{-3}$	$d_1 \cdot 10$	$d_2 \cdot 10^{-3}$
I-4	1	261	154	2.38±0.08	1.44±0.08	-0.04±6	9±6		
	2	278	11.3	2.37±0.09	1.45±0.09)	0.3±3	7±3		
	3	300	4.17	2.37±0.09	1.45±0.09	0.6±2	6±2		
I-5	1	250	2.58	2.39±0.08	1.44±0.09			-2±6	7±6
	2	257	1.62	2.39±0.09	1.45±0.09			-2±3	4±3
	3	269	0.929	2.4±0.4	1.4±0.3			-1.9±1.5	3±1

Table 5. Frequency factor, activation energy adsorption enthalpy and entropy differences between DNOE and 1-octanol, and water and 1-octanol, respectively, for I-4 and I-5 models.

Model type	I-4			I-5		
n	1	2	3	1	2	3
A, $mol \cdot h^{-1} \cdot kg_{cat}^{-1}$	$4 \cdot 10^{15}$	$5 \cdot 10^{15}$	$5 \cdot 10^{15}$	$4 \cdot 10^{15}$	$4 \cdot 10^{15}$	$5 \cdot 10^{15}$
E_a, $kJ \cdot mol^{-1}$	120±7	120±7	120±8	120±7	120±7	120±27
$\Delta S_{a,DNOE} - \Delta S_{a,OcOH}$, $J \cdot mol^{-1} \cdot K^{-1}$	182±115	134±63	134±63			
$\Delta H_{a,DNOE} - \Delta H_{a,OcOH}$, $kJ \cdot mol^{-1}$	78±49	113±45	48±19			
$\Delta S_{a,H2O} - \Delta S_{a,OcOH}$, $J \cdot mol^{-1} \cdot K^{-1}$				130±113	82±61	62±26
$\Delta H_{a,H2O} - \Delta H_{a,OcOH}$, $kJ \cdot mol^{-1}$				57±49	36±26	27±11

Table 6. Correction factors for $\hat{k}'$ tested to represent the water inhibiting effect on the reaction rate.

Equation	Water isotherm	Correction factor	Reference
15	$\theta_{H2O} = \frac{K_{H2O}\sqrt{a_{H2O}}}{1 + K_{H2O}\sqrt{a_{H2O}}}$	$f(a_{H2O}) = \frac{1}{1 + K_{H2O}\sqrt{a_{H2O}}}$	42
16	$\theta_{H2O} = \frac{K_{H2O}a_{H2O}}{1 + K_{H2O}a_{H2O}}$	$f(a_{H2O}) = \frac{1}{1 + K_{H2O}a_{H2O}}$	43
17	$\theta_{H2O} = \frac{K_{H2O}a_{H2O}^2}{1 + K_{H2O}a_{H2O}^2}$	$f(a_{H2O}) = \frac{1}{1 + K_{H2O}a_{H2O}^2}$	44
18	$\theta_{H2O} = \frac{K_{H2O}a_{H2O}^z}{1 + K_{H2O}a_{H2O}^z}$	$f(a_{H2O}) = \frac{1}{1 + K_{H2O}a_{H2O}^z}$	This work
19	$\theta_{H2O} = K_{H2O}a_{H2O}^{1/\propto}$ with $\propto = \frac{K_\propto}{T}$	$f(a_{H2O}) = 1 - K_{H2O}a_{H2O}^{1/\propto}$	41

Table 7. Parameters, frequency factors (A), activation energies (E_a) and enthalpies and entropies differences for model I-5 with n=1 (equation 13), and model I-1 with n=1 with correction factors defined by equations 17, 18 and 19.

		Model I-1(n=1) with correction factor defined by		
	Model I-5(n=1)	Equation 17	Equation 18	Equation 19
a_1	2.79±0.07	2.8±0.1	2.76±0.05	2.79±0.05
a_2	$(1.37\pm0.08)\cdot10^4$	$(1.4\pm0.1)\cdot10^4$	$(1.35\pm0.07)\cdot10^4$	$(1.32\pm0.06)\cdot10^4$
b_1	-0.5±0.6	-	-	-
b_2	$(10\pm7)\cdot10^3$	-	-	-
$K_{H2O,1}$	-	1.2±0.6	2.4±0.8	0.5±0.4
$K_{H2O,2}$	-	$(9\pm8)\cdot10^3$	$(8\pm7)\cdot10^3$	$(3\pm3)\cdot10^3$
K_α	-	-	-	272±49
z	-	-	3.2±0.6	-
A ($mol\cdot h^{-1}\cdot kg^{-1}$)	$7\cdot10^{14}$	$6\cdot10^{15}$	$5\cdot10^{14}$	$3\cdot10^{14}$
E_a ($kJ\cdot mol^{-1}$)	114±7	113±11	113±5	110±5
$\Delta S_{H2O} - \Delta S_{OcOH}$ ($J\cdot mol^{-1}\cdot K^{-1}$)	194±127	-	-	-
$\Delta H_{H2O} - \Delta H_{OcOH}$ ($kJ\cdot mol^{-1}$)	86±55	-	-	-
RSSQ	1301	1095	997	962
Δ RSSQ (%)[a]	-	74.5	76.8	77.6
RSSQRE	1.41	0.977	0.991	1.15

Table 8. Activation energy for DNOE synthesis. Comparison with literature data

Reaction	Catalyst	E_a (kJ·mol^{-1})	Ref
$2(1-\mathrm{OcOH}) \rightleftharpoons \mathrm{DNOE} + \mathrm{H_2O}$	Amberlyst 70	110±6	This work[(a)]
	Amberlyst 70	110±5	This work[(b)]
	Amberlyst 70	99	50
	CT 482	100	50
	H-Beta	150±12	18
$2(1-\mathrm{BuOH}) \rightleftharpoons \mathrm{DNBE} + \mathrm{H_2O}$	Amberlyst 70	122±2	49
$2(1-\mathrm{PeOH}) \rightleftharpoons \mathrm{DNPE} + \mathrm{H_2O}$	Amberlyst 70	114±0.1	26
$2(1-\mathrm{HeOH}) \rightleftharpoons \mathrm{DNHE} + \mathrm{H_2O}$	Amberlyst 70	121±3	27

(a) Estimated from equation 21. (b) From Arrhenius plot of initial rates of DNOE synthesis

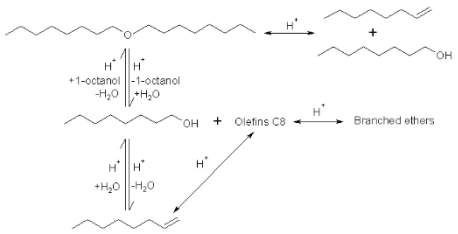

Figure 1. Reaction scheme in the dehydration of 1-octanol to DNOE

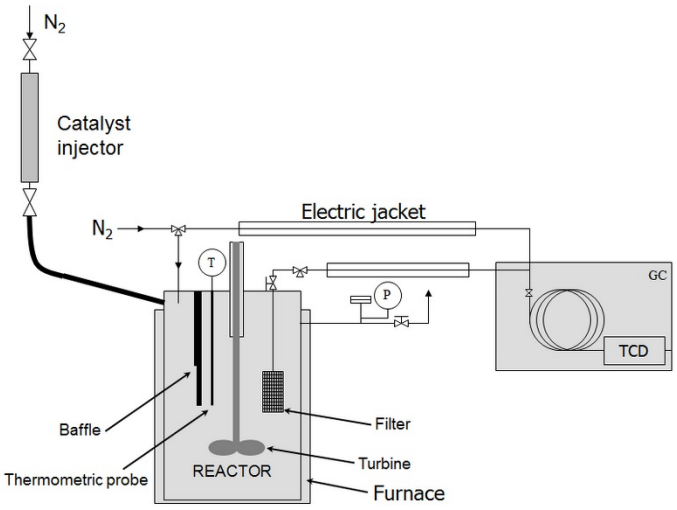

Figure 2. Experimental Setup

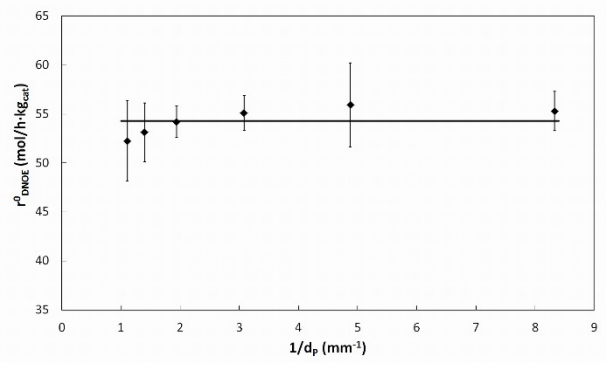

Figure 3. Influence of bead size on initial DNOE formation rate. (70 cm^3 1-octanol, W = 1 g, T = 453 K, N = 500 rpm). Error bars indicate the confidence interval at a 95%-probability level

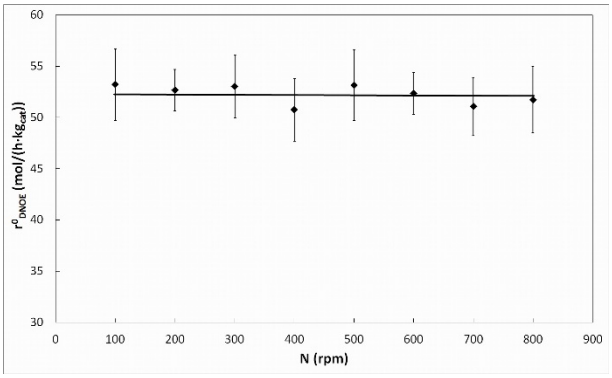

Figure 4. Influence of stirring speed (N) on initial DNOE formation rate (70 cm^3 1-octanol, W = 1 g, $d_{p,m}$ = 0.57 mm, T = 453 K). Error bars indicate the confidence interval at a 95%-probability level.

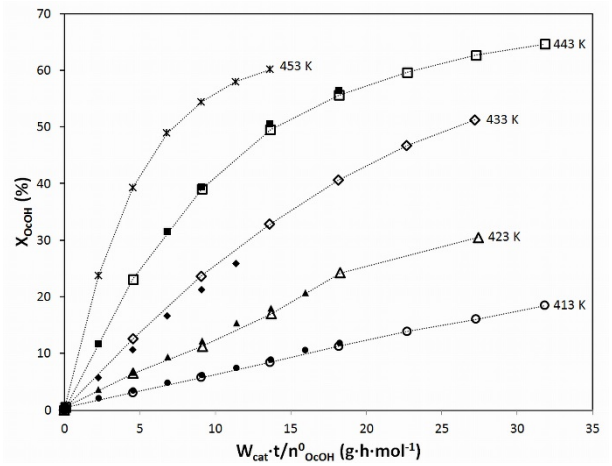

Figure 5. 1-Octanol conversion against contact time. 70 cm^{3}of 1-octanol, W = 1-2 g, $d_{p,m}$ = 0.57 mm, N =500 rpm, W = 1 (solid symbols) or 2 (open symbols) g.

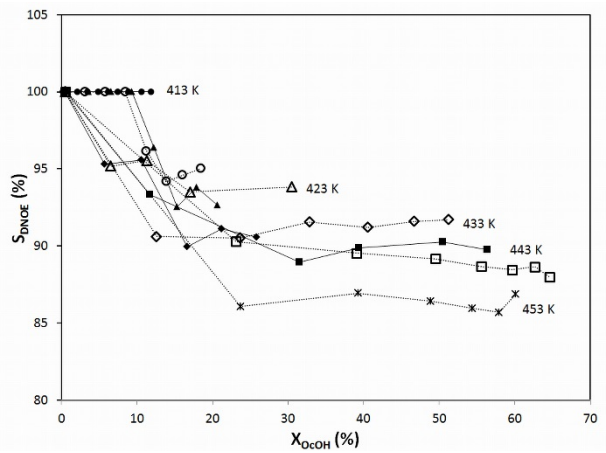

Figure 6. Selectivity to DNOE vs. conversion of 1-octanol. 70 $cm^3$of 1-octanol, W = 1-2 g, $d_{p,m}$ = 0.57 mm, N =500 rpm, W = 1 (solid symbols) or 2 (open symbols) g.

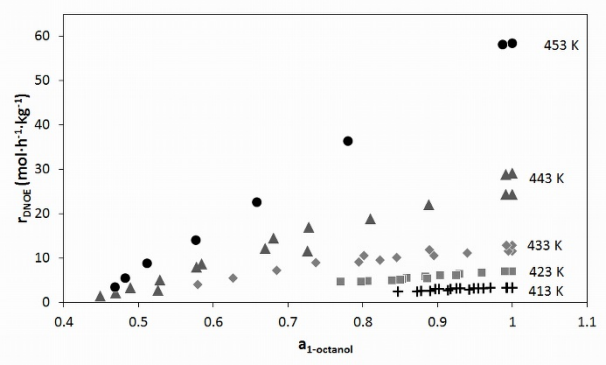

Figure 7. Reaction rates of DNOE formation vs. 1-octanol activity at 413 K (+), 423 K (■), 433 K (♦), 443 K (▲), 453 K (●). 70 $cm^3$of 1-octanol, W = 1-2 g, $d_{p,m}$ = 0.57 mm, N =500 rpm.

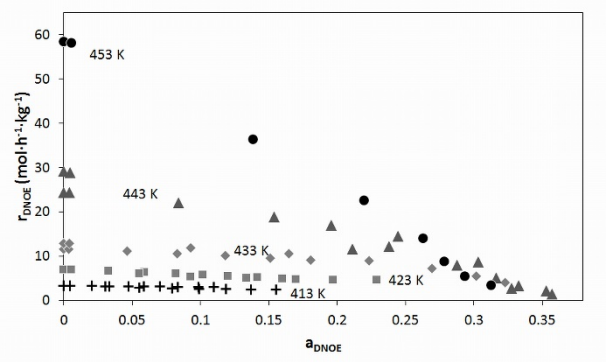

Figure 8. Reaction rates of DNOE formation vs. DNOE activity at 413 K (+), 423 K (■), 433 K (♦), 443 K (▲), 453 K (●). 70 $cm^3$of 1-octanol, W = 1-2 g, $d_{p,m}$ = 0.57 mm, N =500 rpm.

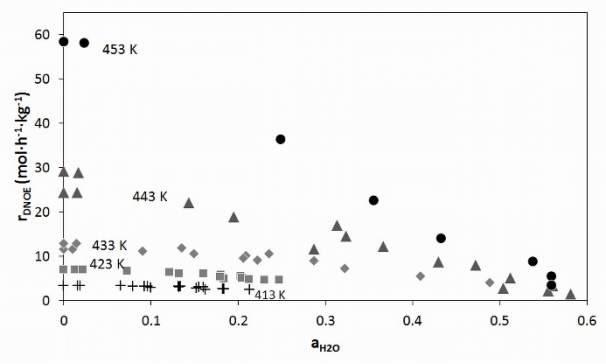

Figure 9. Reaction rates of DNOE formation vs. water activity at 413 K (+), 423 K (■), 433 K (♦), 443 K (▲), 453 K (●). 70 $cm^3$of 1-octanol, W = 1-2 g, $d_{p,m}$ = 0.57 mm, N =500 rpm.

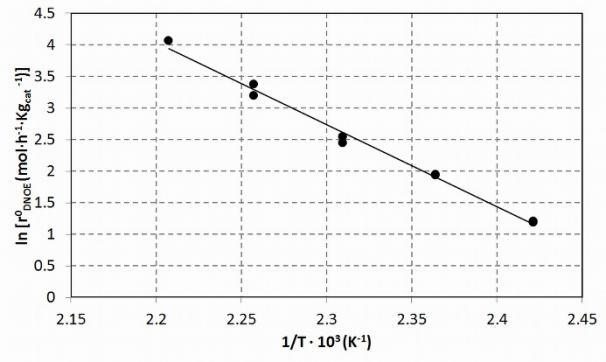

Figure 10. Arrhenius plot for initial DNOE formation rate (W = 1-2 g, $d_{p,m}$ = 0.57 mm, T = 413-453 K, N = 500 rpm).

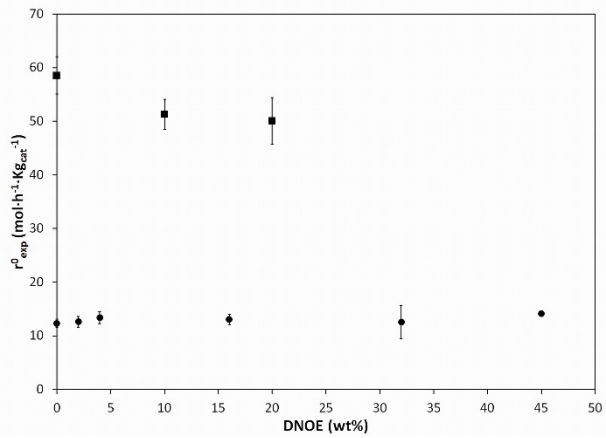

Figure 11. Influence of initial DNOE amount (% wt) on initial reaction rate of DNOE formation at 453K (■) and 433K (●) (70 cm^3 of 1-octanol/DNOE mixture, W = 1 g, $d_{p,m}$ = 0.57 mm, N = 500 rpm). Error bars indicate the confidence interval at a 95%-probability level

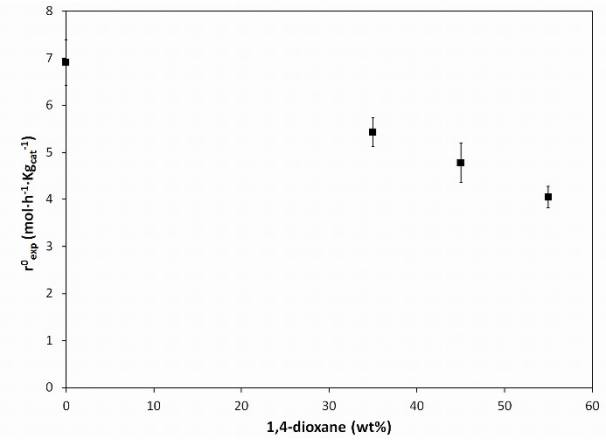

Figure 12. Effect of 1,4-dioxane amount (wt%) on initial reaction rate of DNOE formation at 423K (70 cm^3 1-octanol/1,4-dioxane mixture, W = 1 g, $d_{p,m}$ = 0.57 mm, N = 500 rpm). Error bars indicate the confidence interval at a 95%-probability level

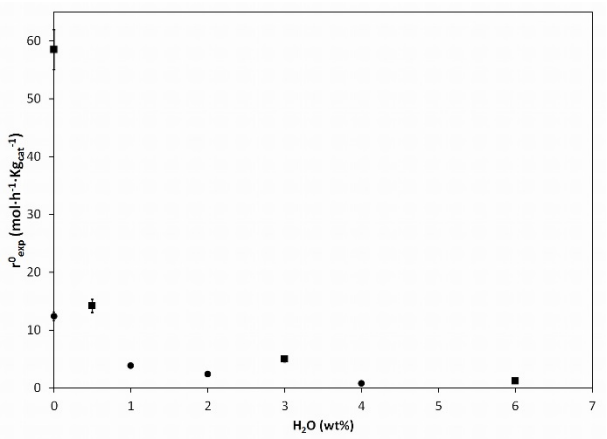

Figure 13. Influence of initial water amount (% wt) on initial reaction rate of DNOE formation at 453K (■) and 433K (●) (70 cm^3 1-octanol/water/1,4-dioxane mixtures, W = 1 g, $d_{p,m}$ = 0.57 mm, N = 500 rpm). Error bars indicate the confidence interval at a 95%-probability level

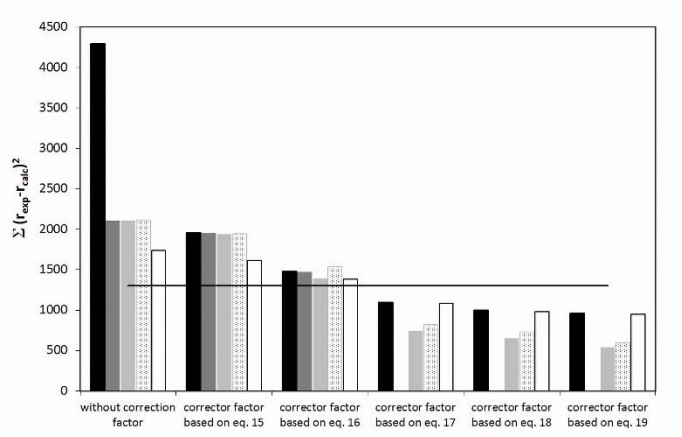

Figure 14. RSSQ for model I-5 with n=1, equation 13 (▬), and models I-1 with n=1 (■), II-1 with n=1 (■) n=2 (■) and n=3 (dotted bar), and I-4 with n=1 (□) with correction factors for inhibitor effect of water based on equations 15-19

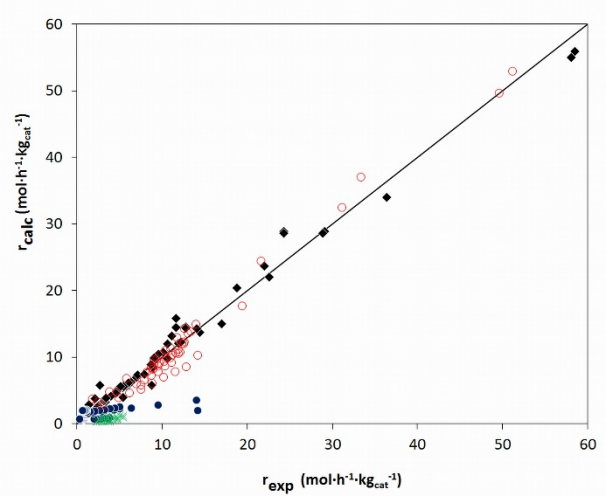

Figure 15. Parity plot for equation 21 (♦, experiments processing only OcOH; o, OcOH-DNOE blends; •, 1,4-dioxane/OcOH/water blends; +, 1,4-dioxane/OcOH blends)

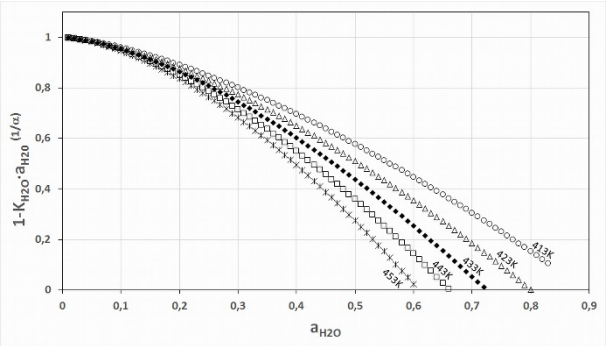

Figure 16. Correction factor for the inhibitory effect of water based on the Freundlich isotherm vs. water activity at different temperatures within the range 413-453K.

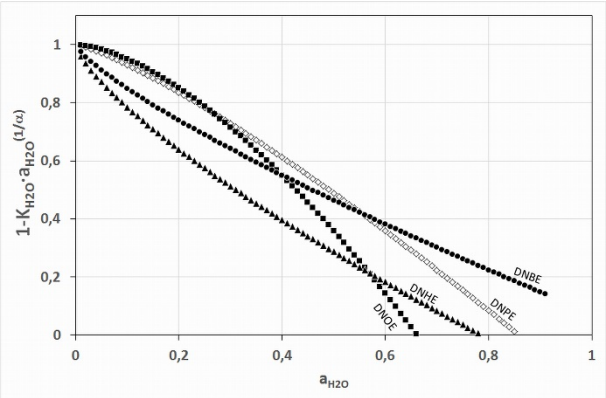

Figure 17. Correction factor for the inhibitory effect of water based on the Freundlich isotherm vs. a_{H2O} in the reactions of synthesis of DNBE, DNPE, DNHE and DNOE, respectively, by dehydration of 1-alkanol at 443 K.